Algorithm for Automatic Scaling of the F-Layer Using Image Processing of Ionograms

Mariano Fagre, *Student, IEEE*, Jose A. Prados, Jorge Scandaliaris, Bruno S. Zossi, Miguel A. Cabrera, Rodolfo G. Ezquer, and Ana G. Elias

***Abstract*— In this article, a method is presented for automatic scaling of the F-layer from ionograms based on an image processing technique for the extraction of curvilinear structures. The algorithm obtains the ordinary and extraordinary traces and determines the F2 critical frequency. The performance was tested using a wide data set of ionograms recorded by the Advanced Ionospheric Sounder/Istituto Nazionale di Geofisica e Vulcanologia (AIS/INGV) ionosonde located at Universidad Nacional de Tucumán, Tucuman, Argentina, and the results are compared with manual scaling and also with Autoscala method. Results from these tests show that the method is feasible and can be the seed for the development of a robust automated scaling system.**

***Index Terms*— F2 critical frequency, image processing, ionogram automatic scaling, ionospheric perturbations.**

I. Introduction

KNOWLEDGE of ionospheric conditions plays a significant role in satellite and terrestrial communications. Extremely important ionospheric characteristics can be extracted from the analysis of ionograms recorded by several sounders deployed around the world that contribute not only to the understanding of the radio propagation in ionized media, physical, and chemical processes in upper atmosphere, ionosphere and magnetosphere coupling, and solar-terrestrial relations but also in the design and operation of different communication systems, such as the case of over the horizon radars (OTHR), which use the ionosphere as a mirror reflector.

Researchers have made many contributions to this field by developing computer programs to automatically scale vertical incidence ionograms. One of the pioneer works is the widely known automatic real-time ionogram scaling with true-height (ARTIST), which needs wave polarization information, and is based on a polynomial approximation using a single sum of Chebyshev polynomials for the F2-layer identification [1]–[3]. To identify F1-layer Galkin *et al.* [4] tested an approach using neural networks. Another well-known program is Autoscala, method developed by Scotto and Pezzopane [5] and Pezzopane and Scotto [6], based on an algorithm of curved fitting by correlation that does not need polarization information, and that identifies and scales the F2-layer [7], [8], E sporadic (Es)-layer [9] and F1-layer [10] traces of the ionograms. An algorithm based on the concepts of fuzzy segmentation and connectedness was developed by Tsai and Berkey [11]. A method implemented on the basis of empirical orthogonal functions in combination with an image matching technique to scale the F2-layer parameters automatically was proposed by Ding *et al.* [12]. The algorithm of Liu *et al.* [13] combines different methods such as fuzzy theory, constraint extrapolations and ARTIST, all based on International Reference Ionosphere (IRI) model. Zheng *et al.* [14] proposed a method that converts ionospheric vertical sounding data to a binary image and extract the F-layer trace through segmentation of the F-layer image. Jiang *et al.* [15], [16] implemented an algorithm using the quasi-parabolic segment model and empirical orthogonal functions to obtain the F2 parameters and F1 critical frequency. Chen *et al.* [17] implemented a method of scaling the F-layer from ionograms automatically which does not need wave polarization information. In Chen *et al.* [18], the sounding data recorded is converted to a gray-level image from which, through preprocessing and binarization, the noise is removed and the F-layer trace is extracted by skeletonization and mathematical morphology. A method to separate the O/X mode for vertical and oblique ionosonde based on direct digital receiver technology and algorithm was developed by Harris *et al.* [19] and Harris and Pedrerick [20].

Despite the progress achieved by the different methods, obtaining high reliability and accuracy from automatic extraction and scaling of ionograms still remains a challenge. Many of the aforementioned techniques to identify the traces present in the ionograms are essentially based on the combination of ionospheric echo signals with empirical and modeled data, using for different fitting and extrapolation methods.

In this article, our goal is the automatic classification of F-layer in ionograms using image processing. This involves both detecting and classifying curves, also referred to as curve tracing, where the aim is identifying, labeling, and following a specific curve across the image even if it intersects with

Manuscript received December 10, 2019; revised April 7, 2020 and May 18, 2020; accepted May 18, 2020. This work was supported by Projects Proyecto de Investigación de la Universidad Nacional de Tucuman (PIUNT) E642 and Proyecto de Investigación Científica y Tecnológica (PICT) 2015-0511. The code is available from Mariano Fagre upon request. *(Corresponding author: Mariano Fagre.)*

Mariano Fagre is with Consejo Nacional de Investigaciones Científicas y Técnicas (CONICET) and Universidad Nacional de Tucumán, Tucumán T4000, Argentina (e-mail: mfagre@herrera.unt.edu.ar).

Jose A. Prados and Miguel A. Cabrera are with Laboratorio de Telecomunicaciones, FACET, Universidad Nacional de Tucumán, Tucumán T4000, Argentina.

Jorge Scandaliaris is with Laboratorio de Técnicas Digitales, FACET, Universidad Nacional de Tucumán, Tucumán T4000, Argentina.

Bruno S. Zossi and Ana G. Elias are with Laboratorio de Física de la Atmosfera, INFINOA (CONICET-UNT), Universidad Nacional de Tucumán, Tucumán T4000, Argentina.

Rodolfo G. Ezquer is with CONICET and Laboratorio de Ionosfera, FACET, Universidad Nacional de Tucumán, Tucumán T4000, Argentina.

Color versions of one or more of the figures in this article are available online at http://ieeexplore.ieee.org.

Digital Object Identifier 10.1109/TGRS.2020.2996405

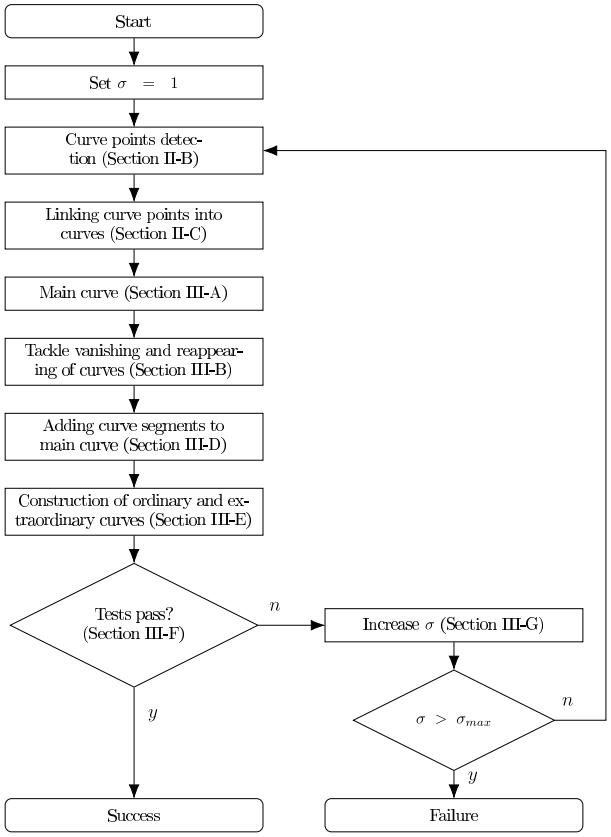

Fig. 1. Method proposed in this article to scale F-layer from ionograms automatically.

another one, and/or fades out and then reappears. To accomplish this, we rely on a method developed by Steger [21] conceived to extract curves and their widths from images with subpixel precision. It is a local method because it determines and classifies if a pixel belongs to a curve or not considering the information from adjacent pixels centered around it. Our method does not need any parameter adjustment because is independent of the ionosonde location, the season, and time. Steger's method consists on three main steps: detection of curve points; linking of curve points into curves; and determination of curve width. Because curve width determination is not of interest for this application, this last step is not applied.

We rely on the information made available from the first two steps and use it to trace the curves associated with the ordinary and extraordinary traces and extract key parameters from them. In the next sections, an overview is given on the parts of Steger's method used here, followed by a detailed description of the modifications added in the last step introduced in this article.

II. Methodology

A. Sounding Data to a Gray-Level Image Conversion

Fig. 1 shows the different steps of the proposed method to scale the F2-layer from ionograms. As a first step, we need to transform the sounding records to grayscale images, as can be seen in Fig. 2(a). Data obtained from Advanced Ionospheric Sounder/Istituto Nazionale di Geofisica e Vulcanologia (AIS/INGV) ionosonde installed at Tucumán [22] are given in binary files which mainly contain echo level received, start, end and step frequencies, as well as minimum, maximum, and resolution heights. These data are transformed into a matrix A with m rows and n columns which represent an ionogram in grayscale with a size of $m \times n$. The values of m and n are given by

$$m = (h_{\max} - h_{\min})/h_{\text{step}} + 1 \quad (1)$$

$$n = (f_{\text{stop}} - f_{\text{start}})/f_{\text{step}} + 1 \quad (2)$$

where f_{step} is the sounding step frequency, the frequency starts from f_{start}, ending in f_{stop}. h_{step} is the height resolution and $h_{\min}$ and $h_{\max}$ are the minimum and maximum height, respectively. The echo amplitude received by the ionosonde is represented in each pixel with a gray-level value, when higher the value, stronger the echo amplitude received. In this article, the grayscale images have a size of 150×381; the intensity of each pixel can be 0, 7 or 15; $f_{\text{start}} = 1.0$ MHz, $f_{\text{stop}} = 20.0$ MHz, $f_{\text{step}} = 0.05$ MHz; $h_{\min} = 90.0$ km, $h_{\max} = 760.5$ km, and $h_{\text{step}} = 4.5$ km.

B. Curve Points Detection

In order to detect each layer trace in an ionogram, we use an image processing method developed by Steger [21] to identify them. Behind Steger's approach is an explicit model for the profile of curves tackled from a differential geometry perspective. The model is developed initially for curves whose profile is a continuous function and has a parabolic shape, and later on extended for the discrete case with bar profiles, both symmetric and asymmetric.

Consider initially the one-dimensional case and a smooth, "rounded" profile, for example, a parabolic profile. The main idea is to consider the profile of a curve as a function $z(x)$. Then, a curve can be detected wherever the first derivative $z'(x)$ vanishes. The second derivative of the profile $z''(x)$ at the point where $z'(x) = 0$ should be of large absolute value, and so it is used as a criterion for detecting salient curves. In the two-dimensional case, curvilinear structures are modeled as curves $s(t)$ having a characteristic 1-D curve profile f_a in the direction perpendicular to the curve, $n(t)$. The first directional derivative in the direction of $n(t)$ should vanish and the second directional derivative should be of large absolute value. In the case of the bar profile, this criterion alone would not be sufficient. However, if the bar profile is convolved with the derivatives of the Gaussian kernel, smooth functions are obtained in all cases. The smoothing effect of the kernel is also beneficial when there is noise present in the images.

To compute the direction of the curve at each point the partial derivatives r_x, r_y, r_{xx}, r_{xy}, and r_{yy} are estimated by convolving the image with discrete two-dimensional Gaussian partial derivative kernels. The direction where the second directional derivative of $z(x, y)$ takes its maximum absolute value, the direction of maximum curvature, is used as the direction of $n(t)$. It can be determined from the eigenvalues and eigenvectors of the Hessian matrix, and specifically from

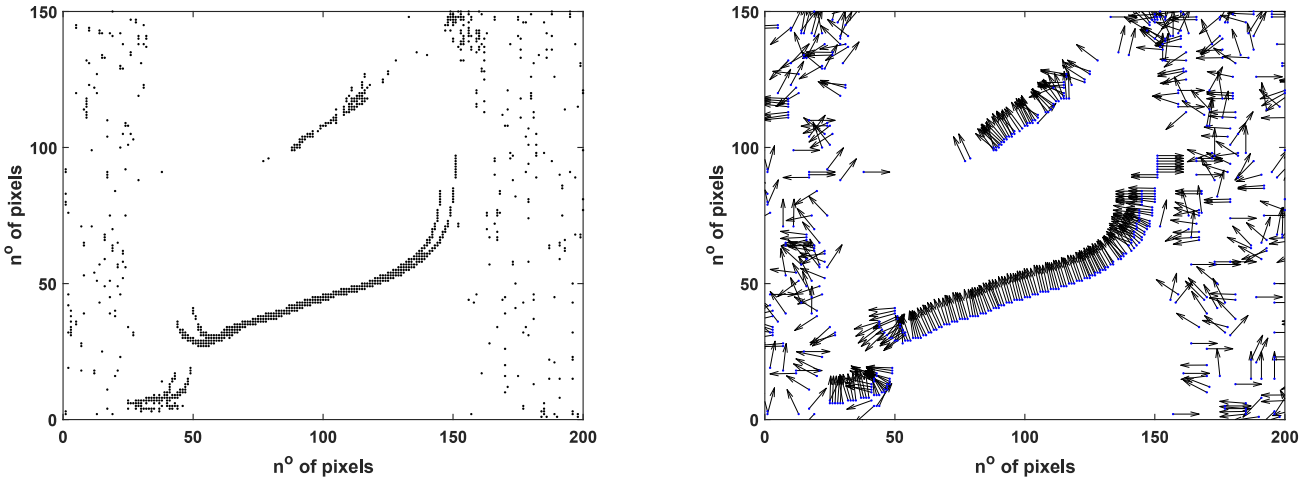

(a) (b)

Fig. 2. (a) Scale-gray conversion of ionogram recorded August 6, 2015, at 20 UT by AIS/INGV sounder located at Universidad Nacional de Tucumán, Argentina. (b) If the subpixel location of the curve lies within the boundaries of the pixel, that is, $(p_x, p_y)\text{in}[-(1/2), (1/2)] \times [-(1/2), (1/2)]$, the pixel is declared as a curve point (blue points) and the black arrows represent the normal vectors $n_{(x,y)}$ of each of the curve points.

the first eigenvector, that associated with the eigenvalue of maximum absolute value

$$H(x, y) = \begin{pmatrix} r_{xx} & r_{xy} \\ r_{yx} & r_{yy} \end{pmatrix}. \tag{3}$$

Let $n = (n_x, n_y)$ be the eigenvector corresponding to the eigenvalue with the maximum absolute value.

Another issue to be addressed in the discrete case is the determination of curve location. Zero crossing detection would only give pixel accuracy. Instead, the function is approximated with a second-order Taylor polynomial $P_T(x, y)$, given that partial derivatives estimates are available

$$P_T(x, y) = r(x, y) + \begin{pmatrix} x & y \end{pmatrix} \begin{pmatrix} r_x \\ r_y \end{pmatrix} + \frac{1}{2} \begin{pmatrix} x & y \end{pmatrix} H \begin{pmatrix} x \\ y \end{pmatrix}. \tag{4}$$

Then one can test whether the derivative along (n_x, n_y) vanishes within the pixel boundaries. This is done by solving for t in $P'_T(tn_x, t\ n_y) = 0$, thereby resulting in

$$t = \frac{r_x n_x + r_y n_y}{r_{xx} n_x^2 + 2 r_{xy} n_x n_y + r_{yy} n_y^2}. \tag{5}$$

The subpixel location of the curve is $(p_x, p_y) = (tn_x, t\ n_y)$. If this lies within the boundaries of the pixel, that is, $(p_x, p_y)\text{in}[-1/2, 1/2] \times [-1/2, 1/2]$, the pixel is declared a curve point. The points that belong to a curve and the corresponding normal vector n are shown in Fig. 2(b).

C. Linking Curve Points Into Curves

From the previous step a list P containing all pixels p that were classified as curve points is available. Also, for each point in P the following data are collected: the orientation of the normal direction $n = (n_x, n_y) = (\cos\alpha, \sin\alpha)$, a measure of strength or saliency of the line (the second directional derivative in the direction of n), referred to as μ from now on, and the subpixel location of the curve (p_x, p_y).

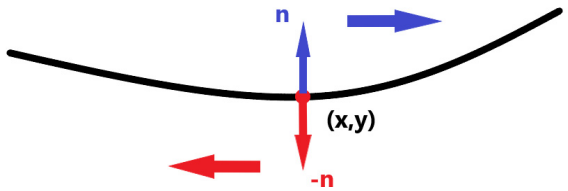

Fig. 3. Maximum value of μ is used as a starting point or seed for the process of linking points into curves, from the list of curve points P. From the seed a search for neighbors is started on the direction of $n^\perp$ (blue arrow pointing to the right) and $-n^\perp$ (red arrow pointing to the left), because the seed will in general lie somewhere in the middle of a curve.

The linking process constructs curves from the curve points detected in the previous step. It starts from the most salient pixel, that is, with the maximum absolute value of μ, which provides a more reliable starting point. From this point, a curve will be generated by adding neighbor points satisfying some criteria. This is done in the direction of $n^\perp$ and $-n^\perp$, as can be seen in Fig. 3, because the initial point will, in general, lie somewhere in the middle of a curve. The search considers three of the eight neighbor pixels depending on the current curve point's direction α (see Fig. 4).

To determine which of them is added to the curve, we consider first if they were classified as curve points, that is, they are in P, and for those that were a metric m is calculated, with $m = d + \beta$, where $d = \|p_2 - p_1\|_2$ is the distance and $\beta = |\alpha_2 - \alpha_1|$ is the angle difference, in radians, between the current point and the candidate under consideration. The candidate that minimizes m is added to the curve. This process is repeated for each added point until no neighbor is found or until the best candidate has already being added to another curve. In the latter case, the point is marked as a junction point, that is, it is added to the set of junction points, J. The curve containing the junction point is split into two curves. New curves are created as long as there are points in P that do not belong to any curve. All curves are kept in a set of curves, C.

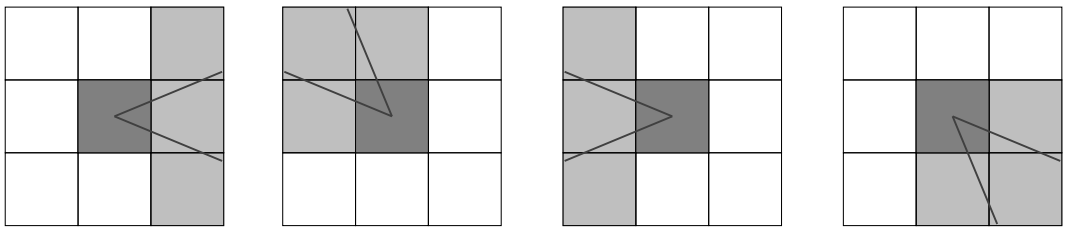

Fig. 4. Search considers three of the eight neighbor pixels depending on the current direction of the curve. Here, we can see four of the eight possible set of three pixels depending on the direction.

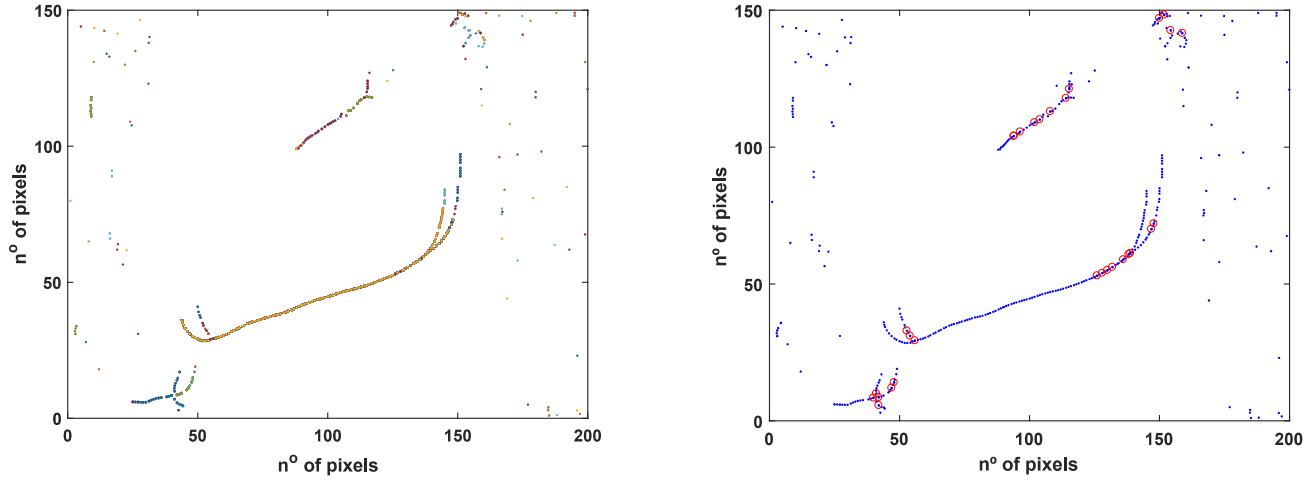

Fig. 5. Results of the linking process applied to the ionogram of Fig. 2(a). (a) During the linking process, new curves are created as long as there are points in the list P that do not belong to any curve. Here, we can see all the segments of curve obtained represented in different colors. (b) All the segments of curve are in blue. During the linking process when the best pixel candidate has already been added to another curve, the point is marked as a junction point (red circles) and the curve is split into two curves.

There is a 180° ambiguity in the determination of the normals. To solve this, we initially assume, when starting from a seed point, a traveling direction for the curve of 0° and that the normal is −90° to this direction, that is, to the right. With subsequent points, we choose the normal direction that minimizes the difference with the previous point. The second part of the curve construction process looks for neighbor points to the seed in the $-n^{\perp}$ direction. To keep the normal directions consistent, the direction that was initially selected for the seed point is kept, and the above mentioned criterion of minimizing the angle difference with the current point continues to be used. This guarantees that as a curve is traversed in a given direction the normal directions will be consistent. Fig. 5(a) shows with different colors the curve segments obtained after the analysis of the ionogram and in Fig. 5(b) we can see all the segments of curves (now in blue) with the intersection points marked by the red circles. These intersection points are the crossing point of two curves.

III. Ordinary and Extraordinary Curves

With the linking process, we obtain a set of all the curves presents in the ionogram under analysis, C, as well as a set of points were some of these curves intersect, J, that is, junction points. The process of determining the ordinary and extraordinary curves from this information is divided into several steps and explained in the sections below.

A. Main Curve

In order to determine the ordinary, O, and extraordinary, X, characteristic curves, we start by looking for the curve with the largest number of points between a predetermined range of virtual height (200–600 km). In our case, this curve is represented by the blue dots in Fig. 6. We are aware that such a choice does not avoid problems related to multiple reflections from both the F-layer and Es-layer, but this is an issue that we are going to address in the future. The multiple echoes of the Es-layer can seriously affect the accuracy of scaling the F-layer. As far as we know, few studies have focused on eliminating or mitigating the effects related to the interference of the multiple reflection and backscatter echoes of the Es-layer for ionograms. Pezzopane and Scotto [7] developed a linear regression-based method to filter out multiple-hop Es-layer echoes. However, if the echoes of the Es-layer are within the mentioned range and the curve presents a number of points greater than the curve of interest, the tool will probably fail. For this first iteration of our tool, we consider that this

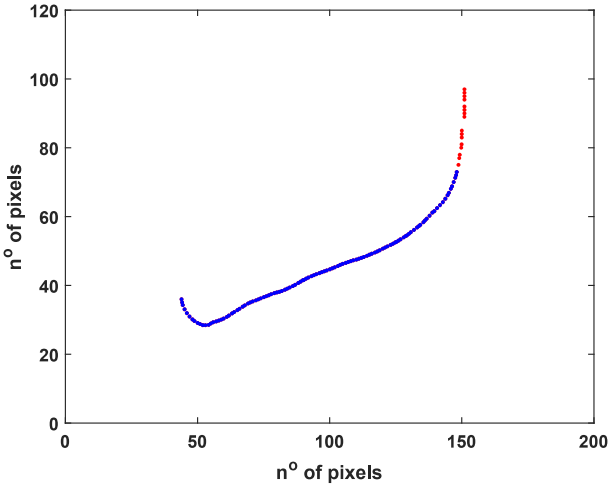

Fig. 6. Reconstruction by vanishing and reappearance of the curve for the ionograms of Fig. 2(a). The *mc* curve is shown in blue and the added sections are in red.

Fig. 7. c_m curve (blue line) vanishes at points (x_1, y_1), (x_3, y_3) and reappears at the points (x_2, y_2) and (x_4, y_4). To effectively determine if the green segment (from (x_4, y_4) to (x_6, y_6)) belongs to the c_m curve, we calculate the distance d between the points (x_3, y_3) and (x_4, y_4), and this means $d = \| (x_3, y_3) - (x_4, y_4) \|_2$. If $d < d_{\text{gap}}$ that we can join the green segment to c_m. The same procedure is applied to the red segment determined by (x_2, y_2) and (x_5, y_5).

ad hoc virtual height range in addition to starting from the curve with the largest number of points is enough to get successful results. In fact, most of the failed detections were not due to the presence of the echoes of the Es-layer. From here on, we refer to this curve, which corresponds to the part of the ionogram where the O and X curves overlap, as the main curve c_m. Before trying to distinguish between the O and X traces we tackle the vanishing and reappearance of curves, a phenomenon usually observed in ionograms due to the ionosonde missing echoes at some frequencies.

B. Vanishing and Reappearing Curves

To solve this issue, we analyze the left end of the c_m, represented by the blue trace in Fig. 7, corresponding to the point (x_3, y_3). In the same figure, we can see how the c_m vanishes and reappears in the point (x_4, y_4) which forms up to the point (x_6, y_6), a green line segment. To effectively determine whether this new segment belongs to the c_m curve, we calculate the distance d between the points (x_3, y_3) and (x_4, y_4), and this means $d = \| (x_3, y_3) - (x_4, y_4) \|_2$. If $d < d_{\text{gap}}$, then we can join the green segment to c_m. A value of 7 was used for d_{gap}. It was obtained after analyzing a great number of ionograms. Let us assume that the condition is satisfied in the example, and then the two curves are joined and the new left end is the point (x_6, y_6). The process is repeated considering the just extended c_m curve, that is, we look for curve segments close to the new endpoint (x_6, y_6). The process finishes when there are no more curves to analyze or none of the analyzed curves satisfy the condition of distance. A similar procedure is used for the right end (point (x_1, y_1)) of the c_m curve. A result of this process is shown in Fig. 6, where the right end of the blue curve vanishes and, after the reconstruction, reappears on the red segments.

C. Junction Points Over the Main Curve

To distinguish between the O and X curves, we need to determine junction points and curve segments associated with c_m. At junction points the two traces depart from each other. Besides junction points found during the classification process described earlier, we add additional ones whenever the distance from c_m to one of the endpoints of the remaining curve segments is smaller than a fixed value, d_{gap}, and the difference in direction between the main curve and the curve segment being considered is below a threshold value. These added junction points take into account possible vanishing of curves near an intersection. The result of this step is a new set of junction points, J_m, which are on the main curve.

D. Adding Curve Segments to the Main Curve

Let p_c be the central point of c_m. We classify all junction points in J_m into two categories: those which lie to the left and those which lie to the right of p_c. Among those to the right, we choose the one associated with the longest curve which also complies with the criterion that all its points have an increasing direction with increasing frequency. If such a curve is found, we also consider if it can be extended (considering possible vanishing effects) following the procedure described before for the c_m curve in Section III-B. For those to the left, we relax the criterion to just the junction point associated with the longest curve, which again is extended if suitable segments are found. Whenever a curve is found either at the left or right of the central point of c_m, the segment past the junction point is split from c_m. A new set of curve segments is created, C_m, which contains the curves found, the curves split from c_m and the central portion of c_m.

E. Construction of Ordinary and Extraordinary Curves From Detected Curve Segments

At this point, depending on the search result for intersections with c_m, there are three possible scenarios:

1) No intersection points were found to either side of the center point of the c_m curve.
2) An intersection point was found to the right of the center point.
3) Intersection points were found at both sides of the center point.

In case 1 above, the result is considered to have failed to trace the curves in the ionograms. In case 2, three curve segments are present in C_m, one where the ordinary and extraordinary curves overlap and two more intersecting the first one, located toward the high frequency range. Let us label the curve segments as follows: The curve segment containing

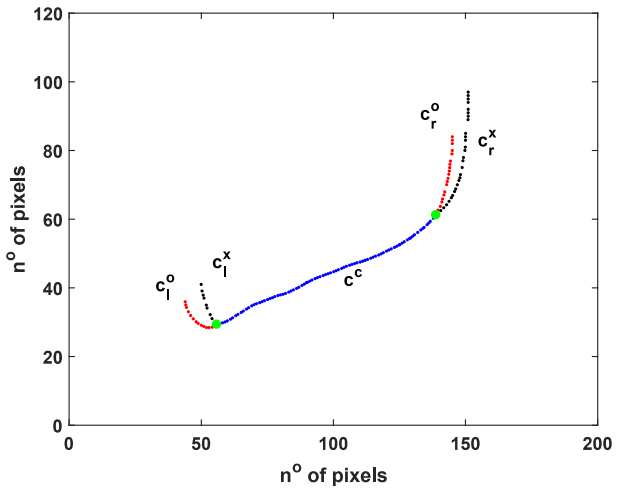

Fig. 8. Final result where O curve is obtained by the intersection of the red and blue segments ($c^o = c_l^o \cup c^c \cup c_r^o$) and the X curve by the intersection of black and blue segments ($c^x = c_l^x \cup c^c \cup c_r^x$). In green are the intersection points.

the central point p_c will be referred to as c_c. The remaining two curve segments start at the right junction point. We compare both segments' right end frequency. That which ends at a higher frequency is labeled as c_r^x and the remaining one as c_r^o. The ordinary curve will then be $c^o = c_c \cup c_r^o$, and the extraordinary curve will be $c^x = c_c \cup c_r^x$. Case 3 can be considered to be the second case plus two additional segments found toward the lower frequency range, that is, toward the left of p_c. From the two additional segments, the one with its left end having the lowest frequency is labeled c_l^o and the other c_l^x. The ordinary curve will be $c^o = c_l^o \cup c^c \cup c_r^o$ and the extraordinary curve will be $c^x = c_l^x \cup c_c \cup c_r^x$. An example of this is shown in Fig. 8.

F. Results Validation

As mentioned earlier, if the search for junction points failed, that is, scenario 1 above, then the method failed in the process of identifying the curves, but that does not strictly mean that the other two cases are successful. There are still a few checks that need to pass for the result to be considered positive. The first has already been mentioned, the search for junction points and associated curves has to lie in scenarios 2 or 3 in Section III-E. The second test verifies that the endpoints' directions, α, for the ordinary and extraordinary curves lie in a certain interval, $30° \leq \alpha \leq 120°$. The third test verifies that the frequency difference between the endpoints of the ordinary and extraordinary curves $\Delta f \leq 0.5$ MHz. The fourth and last check is the virtual height comparison between the ordinary and extraordinary curves at foF2, it must hold that $O_{\text{foF2}} < X_{\text{foF2}}$.

G. Scale Space Search

The steps described in Sections II-B through III-F are performed initially for a σ (the standard deviation present on the Gaussian kernel) value of 1 which we found empirically to give the best results. This value also complies with the requirement that $\sigma \geq (w/\sqrt{3})$, where 2 w is the linewidth. Considering that the width of curves in ionograms varies from a minimum of one pixel to several pixels wide, the default value selected for σ should be adequate for lines up to ≈ 3.4 pixels wide. We are aware of the fact that this could be a problem when the ionogram is characterized by spread-F phenomena, but this is an issue we are going to address in future versions of our code. In this first approach, in those cases where the process is not successful we proceed to repeat it with another, bigger value for σ in increments of 0.1 up to a maximum value of 3. This search in scale space is stopped whenever a good result is achieved.

IV. Results and Discussion

To test the performance of the proposed method, we analyzed 3255 randomly selected ionograms recorded by the AIS/INGV ionosonde installed at Universidad Nacional de Tucumán, Tucuman, Argentina [22] in different seasons and time of 2016 and 2017. The data set includes ionograms in different conditions without any classification or filtering, and was automatically scaled by our method and Autoscala, and manually scaled by an experienced operator. In this article, we use a range of error within $\pm 5\Delta$ (where Δ is the reading accuracy and $\Delta = 0.1$ MHz) respect to the manual result, which is in line with the Union Radio-Scientifique Internationale (URSI) limits of $\pm 5\Delta$ [6].

The ionograms for each full day at one hour interval were processed in a ten-year-old notebook equipped with a first generation Intel Core i5 cpu (Intel Core i5 M 450 running at 2.4 GHz). The average runtime for each ionogram was 16.5 s (with a minimum of 5.2 s and a maximum of 43 s), and the average number of iterations was 4.5 (with a minimum of 1 and a maximum of 31). These values are similar to those obtained for Autoscala with a processing time of approximately 50 s on a computer with 1.60-GHz processor and 512 MB of RAM [22]. We can see that in our case the runtimes are not constant, and this is due mainly, but not exclusively, to the variable number of iterations with varying σ values. As explained before, when the verification criteria is not met, σ is increased and the algorithm is run again until a good result is obtained or a maximum value for σ is reached. This results in a range of possible iterations that goes from 1 to 31.

Table I shows the different confidence levels for daytime and nighttime ionograms to evaluate the performance of our method and Autoscala versus the manually scaled results of foF2 [23], [24]. We can see that the proposed method shows good results for the confidence levels from 1.0Δ to 5.0Δ with percentages of correct scaled ionograms over 70% for daytime and 60% for nighttime and reaching 94.9% for daytime and 90.1% for nighttime, respectively. There is a good agreement between our results and those obtained with Autoscala.

The main factors that can affect the accuracy of the automatic scaling in the confidence levels of 0.0Δ and 0.5Δ are the data set [25] and the method used to perform the analysis. The quality of the ionograms is usually affected by the presence of ionospheric disturbances such as spread F which can manifest as frequency spread-F (FSF), ionogram traces represent irregularities located near the F region peak, range spread-F (RSF), ionogram traces located mainly at the bottomside of the F region, mixed spread-F (MSF),

TABLE I

CORRECT RATE OF foF2 EXTRACTED VALUES IN THE DIFFERENT CONFIDENCE LEVELS FOR DAYTIME AND NIGHTTIME IONOGRAMS. THIS TABLE PRESENTS THE RESULTS OF THE COMPARISON BETWEEN THE PROPOSED METHOD VERSUS MANUALLY SCALED IONOGRAMS AND AUTOSCALA METHOD VERSUS MANUALLY SCALED IONOGRAMS

Confidence level	Our Meth. vs Man.		Our Meth. vs Man.(%)		Autosc. vs Man.		Autosc. vs Man.(%)	
	Day	Night	Day	Night	Day	Night	Day	Night
0.0Δ	527	288	30.4	18.41	1432	1095	82.7	70.0
0.5Δ	813	624	47.0	39.9	1457	1122	84.2	71.7
1.0Δ	1327	1014	76.7	64.8	1500	1177	86.6	75.3
1.5Δ	1504	1196	86.9	76.5	1533	1196	88.6	76.5
2.0Δ	1553	1257	89.7	80.4	1614	1314	93.2	84.0
2.5Δ	1573	1299	90.8	83.0	1635	1323	94.5	84.6
5.0Δ	1641	1409	94.9	90.1	1681	1435	97.1	91.8

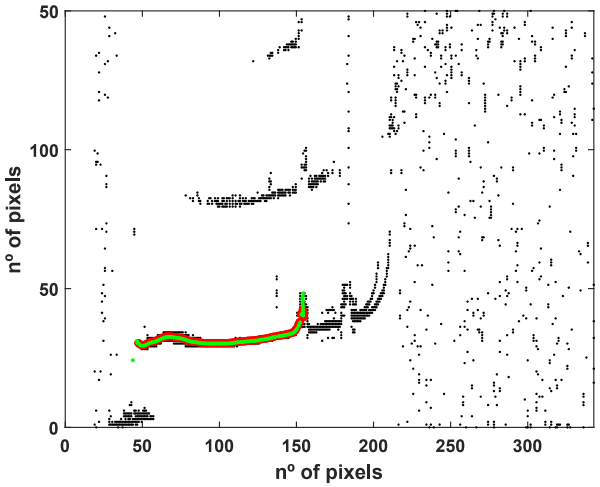

Fig. 9. Ionogram whose scaling failed. Black dots represent the original ionograms, green dots correspond to ordinary trace, and red dots to extraordinary trace.

ionogram traces located throughout the F region, strong range spread-F (SSF), ionogram traces are instead characterized by an extended range spread-F echo that significantly extends well past the critical frequency foF2 of the F region, covering the whole ionosonde frequency range. The ionosonde used in this article is located under the south crest of the equatorial ionization anomaly (EIA), region which presents a strong variability [26]. Even with a weak presence of irregularities the performance of the automatic scaling could be strongly affected due to the vanishing of the curves or the appearance of point clouds around the F2 region making the foF2 detection more difficult. In Fig. 9, we can see an example of an ionogram whose scaling failed.

V. CONCLUSION

This article is mainly focused on the automatic scaling of the critical frequency foF2 of the F2-layer from ionograms recorded by the AIS/INGV ionosonde located at the Universidad Nacional de Tucumán, Tucuman, Argentina. The performance was analyzed by comparison with manual scaling and Autoscala. The results are promising, suggesting that our method could be the seed for the development of a robust automated scaling system. The main advantage of the proposed method is that it is completely independent of the ionosonde station, location, season, and time. Besides, the program was designed to scale the ionograms without using information on polarization and can be applied to both single and crossed antenna systems. Despite these good initial results, we identified a couple of areas where we believe there is room for improvement and we have some ideas we intend to explore: First, Steger's is a local method, and we believe it could benefit from the use of some global features; second, the use of an adaptive value of σ for different portions of the curves; and last, the heuristics employed for the construction of the ordinary and extraordinary curves need to be both augmented to cover more specific cases and tested with ionograms from other sites.

REFERENCES

[1] X. Huang and B. W. Reinisch, "Automatic calculation of electron density profiles from digital ionograms 2. True height inversion of topside ionograms with the profile-fitting method," *Radio Sci.*, vol. 17, no. 4, pp. 837–844, Jul./Aug. 1982, doi: 10.1029/RS017i004p00837.

[2] I. A. Galkin and B. W. Reinisch, "The new ARTIST 5 for all digisondes," Ionosonde Netw. Advisory Group Bull. 69, IPS Radio Space Services, Surry Hills, NSW, Australia, Tech. Rep., 2008, pp. 1–8. [Online]. Available: http://www.ips.gov.au/IPSHosted/INAG/web-69/2008/artist5-inag.pdf

[3] B. W. Reinisch and H. Xueqin, "Automatic calculation of electron density profiles from digital ionograms: 3. Processing of bottomside ionograms," *Radio Sci.*, vol. 18, no. 3, pp. 477–492, May 1983, doi: 10.1029/rs018i003p00477.

[4] I. A. Galkin, B. W. Reinisch, G. A. Ososkov, E. G. Zaznobina, and S. P. Neshyba, "Feedback neural networks for ARTIST ionogram processing," *Radio Sci.*, vol. 31, no. 5, pp. 1119–1128, Sep. 1996.

[5] C. Scotto and M. Pezzopane, "A software for automatic scaling of foF2 and MUF(3000)F2 from ionograms," in *Proc. 27th Gen. Assem. Int. Union Radio Sci.*, Maastricht, The Netherlands: International Union of Radio Science, Ghent, CD-ROM, Aug. 2002, pp. 17–24.

[6] M. Pezzopane and C. Scotto, "The INGV software for the automatic scaling of foF2 and MUF(3000)F2 from ionograms: A performance comparison with ARTIST 4.01 from Rome data," *J. Atmos. Solar-Terr. Phys.*, vol. 67, no. 12, pp. 1063–1073, Aug. 2005.

[7] M. Pezzopane and C. Scotto, "Highlighting the F2 trace on an ionogram to improve autoscala performance," *Comput. Geosci.*, vol. 36, no. 9, pp. 1168–1177, Sep. 2010.

[8] C. Scotto and M. Pezzopane, "Removing multiple reflections from the F2 layer to improve autoscala performance," *J. Atmos. Solar-Terr. Phys.*, vol. 70, no. 15, pp. 1929–1934, Dec. 2008.

[9] C. Scotto and M. Pezzopane, "A method for automatic scaling of sporadic E layers from ionograms," *Radio Sci.*, vol. 42, no. 2, pp. 1–5, Apr. 2007.

[10] M. Pezzopane and C. Scotto, "A method for automatic scaling of F1 critical frequencies from ionograms," *Radio Sci.*, vol. 43, no. 2, pp. 1–12, Apr. 2008.

[11] L.-C. Tsai and F. T. Berkey, "Ionogram analysis using fuzzy segmentation and connectedness techniques," *Radio Sci.*, vol. 35, no. 5, pp. 1173–1186, Sep. 2000.
[12] Z. Ding, B. Ning, W. Wan, and L. Liu, "Automatic scaling of F2-layer parameters from ionograms based on the empirical orthogonal function (EOF) analysis of ionospheric electron density," *Earth, Planets Space*, vol. 59, no. 1, pp. 51–58, Jan. 2007.
[13] W. Liu, Q. Kong, Y. Chen, and J. Fan, "Method on ionogram autoscaling based on IRI model," *Chin. J. Radio Sci.*, vol. 24, no. 2, pp. 218–223, 2009.
[14] H. Zheng, G. Ji, G. Wang, Z. Zhao, and S. He, "Automatic scaling of F layer from ionograms based on image processing and analysis," *J. Atmos. Solar-Terr. Phys.*, vols. 105–106, pp. 110–118, Dec. 2013, doi: 10.1016/j.jastp.2013.09.007.
[15] C. Jiang, G. Yang, Z. Zhao, Y. Zhang, P. Zhu, and H. Sun, "An automatic scaling technique for obtaining F2 parameters and F1 critical frequency from vertical incidence ionograms," *Radio Sci.*, vol. 48, no. 6, pp. 739–751, Nov. 2013, doi: 10.1002/2013RS005223.
[16] C. Jiang *et al.*, "Improvement of automatic scaling of vertical incidence ionograms by simulated annealing," *J. Atmos. Solar-Terr. Phys.*, vol. 133, pp. 178–184, Oct. 2015, doi: 10.1016/j.jastp.2015.09.002.
[17] Z. Chen, S. Wang, G. Fang, and J. Wang, "Ionograms denoising via curvelet transform," *Adv. Space Res.*, vol. 52, no. 7, pp. 1289–1296, Oct. 2013, doi: 10.1016/j.asr.2013.07.004.
[18] Z. Chen, Z. Gong, F. Zhang, and G. Fang, "A new ionogram automatic scaling method," *Radio Sci.*, vol. 53, pp. 1149–1164, Sep. 2018, doi: 10.1029/2018RS006574.
[19] T. J. Harris, M. A. Cervera, L. H. Pederick, and A. D. Quinn, "Separation of O/X polarization modes on oblique ionospheric soundings," *Radio Sci.*, vol. 52, no. 12, pp. 1522–1533, Dec. 2017, doi: 10.1002/2017RS006280.
[20] T. J. Harris and L. H. Pederick, "A robust automatic ionospheric O/X mode separation technique for vertical incidence sounders," *Radio Sci.*, vol. 52, no. 12, pp. 1534–1543, Dec. 2017, doi: 10.1002/2017RS006279.
[21] C. Steger, "An unbiased detector of curvilinear structures," *IEEE Trans. Pattern Anal. Mach. Intell.*, vol. 20, no. 2, pp. 113–125, 2nd Quart., 1998.
[22] M. Pezzopane *et al.*, "The new ionospheric station of Tucumán: First results," *Ann. Geophys.*, vol. 50, no. 3, 483–492, 2007.
[23] C.-F. Enell *et al.*, "Comparison between manual scaling and autoscala automatic scaling applied to Sodankylä geophysical observatory ionograms," *Geosci. Instrum., Methods Data Syst.*, vol. 5, no. 1, pp. 53–64, Mar. 2016.
[24] M. Pezzopane, V. G. Pillat, and P. R. Fagundes, "Automatic scaling of critical frequency foF2 from ionograms recorded at São José dos Campos, Brazil: A comparison between autoscala and UDIDA tools," *Acta Geophysica*, vol. 65, no. 1, pp. 173–187, Mar. 2017.
[25] L. F. McNamara, J. M. Retterer, M. A. Abdu, I. S. Batista, and B. W. Reinisch, "F2 peak parameters, drifts and spread F derived from digisonde ionograms for the COPEX campaign in Brazil," *J. Atmos. Solar-Terr. Phys.*, vol. 70, nos. 8–9, pp. 1144–1158, Jun. 2008.
[26] L. Alfonsi *et al.*, "Comparative analysis of spread-F signature and GPS scintillation occurrences at Tucumán, Argentina," *J. Geophys. Res., Space Phys.*, vol. 118, no. 7, pp. 4483–4502, Jul. 2013, doi: 10.1002/jgra.50378.

Mariano Fagre (Student, IEEE) was born in Argentina in 1987. He received the electronic engineer degree from the Universidad Nacional de Tucumán (UNT), Tucumán, Argentina, in 2013, where he is a Ph.D. student, Consejo Nacional de Investigaciones Cientificas y Tecnicas (CONICET) fellow, and graduate teaching assistant of electronic. His main area of research is ionospheric radio propagation in quiet and perturbed conditions and ionospheric perturbations modeling.

Jose A. Prados was born in Argentina in 1990. He received the electronic engineer degree from the Universidad Nacional de Tucumán (UNT), Tucumán, Argentina, in 2017. His research interests include image processing, tracking and detection and high frequency (HF) high stability amplifiers design.

Jorge Scandaliaris graduated as an electronics engineer from the Universidad Nacional de Tucumán (UNT), Tucumán, Argentina, in 1997 and obtained the Diploma de Estudios Avanzados (DEA) from Technical University of Catalonia (UPC), Barcelona, Spain, in 2007. Now, he works as an Adjunct Professor of digital electronics at UNT. He is experienced in digital design and computer vision. His research interests include color constancy, tracking and detection, and programmable logic devices.

Bruno S. Zossi was born in Argentina in 1989. He received the bachelor degree in physics from the Universidad Nacional de Tucumán (UNT), Tucumán, Argentina, in 2016, where he is a Ph.D. student, Consejo Nacional de Investigaciones Cientificas y Tecnicas (CONICET) fellow, and graduate teaching assistant of statistical physics. His area of research is the secular variation of the Earth's magnetic field and its effects on the upper atmosphere and magnetosphere.

Miguel A. Cabrera was born in Neuquén, Argentina. He received the Ph.D. degree in physics from the Universidad Nacional de Tucumán (UNT), Tucumán, Argentina, in 2003. His research interests include subionospheric and transionospheric radiopropagation and radar technologies.

Rodolfo G. Ezquer received the Ph.D. degree in physics from the Universidad Nacional de Tucumán (UNT), Tucumán, Argentina, in 1991. His research interests include ionospheric electron density modeling and subionospheric and transionospheric radiopropagation.

Ana G. Elias received the Ph.D. degree in physics from the Universidad Nacional de Tucumán (UNT), Tucumán, Argentina, in 1999, where she works as a Researcher from the Consejo Nacional de Investigaciones Cientificas y Tecnicas (CONICET) and as a Professor of statistical physics. Her research is mainly focused in Earth's magnetic field secular variations and reversal scenarios, ionosphere long-term trends and its connection to Earth's magnetic field and radiowave propagation.